JOURNAL OF APPLIED ELECTROCHEMISTRY 26 (1996) 72–82

Oxygen evolution and hypochlorite production on Ru–Pt binary oxides

C.-C. HU, C.-H. LEE, T.-C. WEN*

Department of Chemical Engineering, National Cheng Kung University, Tainan, Taiwan 70101, Republic of China

Received 2 February 1995; revised 2 July 1995

The electrocatalytic activities of Ru–Pt binary oxide electrodes prepared by thermal decomposition for both oxygen and chlorine evolution reactions (OER and CER) were investigated by cyclic voltammetry (CV) and log i/E relationships (Tafel study). Both CV and Tafel studies revealed that the electrodes from the coating solutions with 60 and 20 mol % Pt content possessed the maximum apparent activity for OER and optimal apparent activity for CER/hypochlorite production, respectively. The specific activity (i/q^*) revealed that mixing of the RuO_2 and PtO_x had no synergistic effects for OER due to the occurrence of phase segregation, which was revealed by element mapping/surface morphologies and Auger electron spectroscopy. Lower current efficiencies for hypochlorite production were found on the freshly prepared binary electrodes (type I electrodes) than on those having been treated by repetitive CVs (type II electrodes). Stability testing of both type I and II electrodes was measured in 0.5 M NaCl solution at 300 mA cm^{-2} for 480 h, indicating that both type I and II electrodes are quite stable under the above conditions.

1. Introduction

The chlorine evolution reaction (CER), based on the direct anodic discharge of Cl^-, is one of the largest industrial process in electrochemisty. Although it is a facile reaction with low activation overpotential [1, 2], the oxygen evolution reaction (OER) is an unavoidable side reaction, especially in low chloride ion concentration and decreases the current efficiency for CER. In addition, hypochlorite, an important oxidizing agent and mediator in water/wastewater treatment and organic synthesis, is formed from chlorine molecules in intermediate and basic solutions via: $Cl_2 + OH^- \rightleftharpoons HClO + Cl^-$ [2–4]. Thus, the development of electrocatalysts for this anodic process is still an interesting topic for electrochemists and engineers.

Several patents [5–8] proposed that noble metal oxides, such as RuO_2, IrO_2, PdO_y, PtO_x, etc., mixed with transition metal oxides (e.g. TiO_2, SnO_2, ZrO_2, etc.) exhibit electrocatalytic activities for both OER and CER. The sequence of noble metal oxides with increasing activation overpotential for CER and OER are shown in sequences (i) and (ii), respectively:

$$Pd \simeq Ru < Ir < Rh < Pt \quad \text{(i)}$$

$$Ru < Ir < Rh < Pd < Pt \quad \text{(ii)}$$

Saito *et al.* [7] claimed that for a mixed Pd–Ru–Sn oxide-coated electrode, palladium increases selectivity for CER. However, our preliminary results suggest that PdO_y was significantly corroded in acidic chloride environments due to the formation of $PdCl_2$ after extensive Cl_2 evolution. In addition, CER is a relatively reversible reaction [1, 2] and its activation overpotential on PtO_x, a more corrosion resistant material in acidic chloride media [9], should be close to that of PdO_y. Therefore, based on the above information, mixed Ru + Pt oxide would seem to be the anodes of choice for CER/hypochlorite production.

The mechanism of CER on Pt was studied by Li *et al.* [10]. Lassali *et al.* [11] studied the change in textural structures of $RuO_2 + TiO_2$ by adding PtO_x. However, the electrochemical activities of this series of mixed ternary oxide electrodes on both OER and CER have not been systematically investigated. The purpose of this work is to study the effect of varying coating solution Pt(Ru) mol % on the abilities of Ru–Pt oxide electrodes to evolve oxygen and to produce hypochlorite. The effects of degree of atomic mixing between Ru and Pt oxides on the electrocatalytic activities for both reactions are also examined and discussed.

2. Experimental detail

2.1. *Electrode preparation*

Oxides of variable composition, x mol % Pt + $(100 - x)$ mol % Ru were coated on a titanium substrate (10 mm × 10 mm × 1.2 mm) by thermal decomposition. The starting solution contained a total concentration of 0.3 M H_2PtCl_6 (Johnson Matthey) and $RuCl_3$ (Johnson Matthey) in isopropanol (Merck GR) solutions with 10% by volume concentrated HCl (Merck GR). The solutions were then repeatedly

* Author to whom correspondence should be addressed.

0021-891X/93

sonicated for 15 min periods in an ultrasonic bath (Branson Ultrasonic Co., USA). The titanium substrates were first degreased with soap and water, etched for 1 h in a 6 M HCl solution at 80–90 °C, then washed with ultrapure water. After drying, the substrates were dipped in their respective isopropanol solutions, dried in air for 30 min at room temperature, and then dried at 85–90 °C in a vacuum furnace for 5–10 min at a reduced pressure of 400 mm Hg. The supports were then fired under air flow at 400 °C for 10 min. Further coatings were applied in a similar manner, a total of eight being used in this work. The final annealing treatment in hot air at 400 °C took one hour. The freshly prepared electrodes (type I electrodes) were doubly coated with epoxy resin and PTFE films and had exposed geometric areas of 1 cm^{-2}. Those electrodes, having been treated by repeated cyclic voltammetry within 0–1.5 V in either 1 M NaOH or 0.5 M H_2SO_4, were denoted as type II electrodes.

2.2. *Material characterization*

The surface morphologies/element mapping of both type I and II electrodes were examined by means of scanning electron microscopy (SEM) (Joel JSM35 SEM). The Auger electron spectroscopy (AES) measurements were performed using a Microlab 310D (VG Scientific Ltd) spectrometer. AES depth profilings were performed at emission currents of 0.1 and 8 mA with gun tensions of 10 (electron) and 3 kV (ion), respectively.

2.3. *Electrochemical characterization*

The electrochemical properties of this series of mixed Ru–Pt oxide electrodes were examined by an Electrochemical Analyzer system, BAS-100B (Bioanalytic System, Inc., USA). The electrochemical characteristics of the type I and II electrodes were examined by cyclic voltammetry and potentiodynamic methods. An Ag/AgCl electrode (Argenthal, 3 M KCl, 0.207 V (SHE) at 25 °C) was used as the reference, while a platinum wire was employed as the counter electrode. A Luggin capillary, whose tip was set at a distance of about 1–2 mm from the surface of the working electrode, was used to minimize errors due to *iR* drop in the electrolytes. All data in this work are reported relative to the reversible hydrogen electrode (RHE).

The hypochlorite production setup comprised a Pyrex jacket cell containing 500 cm^{-3} 0.5 M NaCl. Hypochlorite was produced at 25 °C with a laboratory d.c. power supply (GPC-3030D, Good Will Instrument Company Limited, Taiwan) set in galvanostatic mode. The anode and cathode (Ti) were fixed at a distance of 3 cm with exposed geometric areas equal to 9 and 9.6 cm^2, respectively. Hypochlorite current efficiency was determined by the iodometric method [12] after 3240 C passed.

Stability testing of both type I and II electrodes were carried out in a 0.5 M NaCl solution, in the same cell for the hypochlorite production at 25 °C, at an anodic current density of 300 mA cm^{-2} for 480 h. The electrolytes for stability testing were renewed every 24 h. The relationship between cell voltage and time was recorded.

All solutions used in this work were prepared with ultrapure water produced by a reagent water system (MILLI-Q SP, Japan) at 18 MΩ cm^{-1}. In addition, the various solutions used for studying the electrochemical behaviour of oxide reduction/oxidation and the electrocatalytic activities for OER and CER on Ru–Pt binary oxide-coated electrodes were degassed before the experiments with purified nitrogen gas for 15 min. This nitrogen gas flowed above the solution during the voltammetric measurements. Solution temperature was maintained at 25 °C (with an accuracy of 0.1 °C) by means of a water thermostat (Haake D8 and G).

3. Results and discussion

3.1. *Cyclic voltammograms*

The cyclic voltammograms of a RuO_2-coated electrode in 0.5 M H_2SO_4 and 1 M NaOH are shown in Fig. 1 as curves 1 and 2, respectively. The voltammetric responses of the RuO_2 obtained in either acidic or basic solutions are similar to those observed by previous workers [9, 13–15]. The features of high background currents and broad peaks on both positive and negative sweeps were discussed previously [13] and were attributed to the surface redox transitions of oxyruthenium (i.e. Ru(III)/Ru(II), Ru(IV)/Ru(III), Ru(VI)/Ru(IV) and Ru(VII)/Ru(VI)). The voltammetric charges of these redox couples have been found to be directly proportional to the electrochemically active surface sites for OER and the hydrogen evolution reaction (HER) [13, 16]. Therefore, the voltammetric charge (q^*) which, for such inert electrolytes as H_2SO_4 and NaOH, is obtained by numerical integration within the potential region located between HER and OER on a cyclic voltammogram, is an

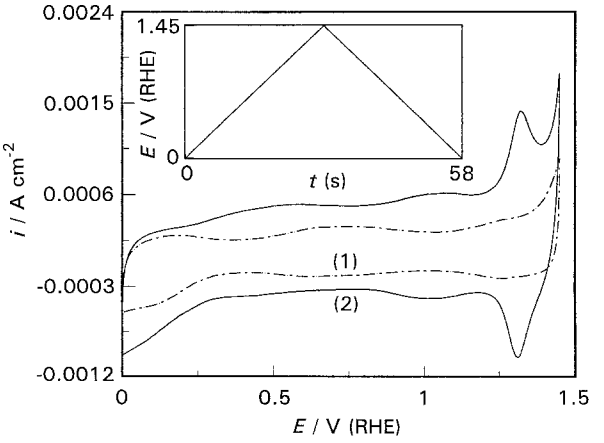

Fig. 1. Cyclic voltammograms at 50 mV s^{-1} for RuO_2 electrodes in (1) 0.5 M H_2SO_4 and (2) 1 M NaOH at 25 °C.

effective index in determining the electrochemically active surface area (EASA) of the RuO_2-coated electrode. The mechanism for redox transitions of the surface oxycations has been proposed as [13, 16, 17, 25]:

$$[MO_a(OH)_b \cdot xH_2O] + \delta H^+ + \delta e^- \rightleftharpoons [MO_{a-\delta}(OH)_{b+\delta} \cdot xH_2O] \quad (1)$$

where surface oxycations exchange H^+ (or OH^-) with the electrolyte solution when electron transfer occurs. The symbol, M, indicates a transition metal such as Ru, Ir, Ni, Co, etc.

The voltammetric behaviour of a type I (freshly prepared) PtO_x-coated electrode investigated in 1 M NaOH is represented in Fig. 2(b) since PtO_x is unstable under cathodic polarization at 0 V in our preliminary study. Moreover, the CV curves did not change after these electrodes were subjected to 6–8 cycles in the 0–1.5 V range. These CV curves of the type II PtO_x-coated electrodes in 0.5 M H_2SO_4 and 1 M NaOH are presented as curves 1 and 2, respectively in Fig. 2(a). In Fig 2(b), the CV diagram, in general, possesses several features of a normal platinum electrode; however, there are some different characteristics on this curve. First, the voltammetric charge in the hydrogen desorption range is much smaller than that in the adsorption range, indicating that a significant amount of platinum oxide is reduced in this negative scan. Secondly, double layer charging between H desorption and oxide formation is not found while currents due to oxide formation are observed. Thirdly, from an examination of the first six CV curves of type I PtO_x electrode (not shown here), voltammetric currents of oxide formation/reduction increased in the first four runs, reached a maximum on the fourth run, then, decreased in the last two runs. Finally, the i/E curve in Fig. 2(a) were obtained. This observation suggest that the platinum oxide is more easily reoxidized and reduced in the first four CV runs because, during oxide reduction, the place-exchange reaction may result in a rougher surface/increase in the population of Pt adatoms on the electrode surface [21].

In Fig. 2(a), the voltammetric response of type I PtO_x electrode is similar in shape to those of a Pt black electrode. An examination of curves 1 and 2 in Fig. 2(a) provides further understanding of the hydrogen adsorption/desorption and platinum oxide formation/reduction. First, three pairs of symmetrical peaks due to the oxidation/reduction of the strongly, weakly adsorbed H species and hydrogen molecules (with respect to decreasing electrode potential) on the Pt surface are clearly observed, in spite of different solution pH values; however, the respective charges in the acidic medium are different from those in the basic electrolyte. Results similar to the above were also found in the literature [18, 19] but not discussed in detail. Secondly, double-layer charging is clearly present in the acidic solution but absent in the basic medium. These results were attributed to the super-Nernstian potential/pH effect for initial formation of the platinum oxide [20, 21]. In addition, this phenomenon is also clearly observed on the Pt black electrode and is attributable to a large population of Pt atoms with low bulk lattice coordination number on the electrode surface [21]. On the other hand, the electronic structure (i.e. d-band) of the platinum clusters with such a high surface/volume ratio may be different from that of a normal bulk Pt lattice [22]. This may result in the oxidative property of this Pt cluster being different from that of normal bulk Pt.

Typical CV diagrams in both H_2SO_4 and NaOH solutions on the Ru + Pt oxide electrode with Pt 60 mol % are shown in Fig. 3. The voltammetric responses of type I and type II electrodes are shown in Fig. 3(b) and 3(a), respectively. In both figures, the voltammetric currents of this electrode are not attributable to the redox transition of the surface oxyruthenium species, since these CV curves are different from that of RuO_2. This is due to the unstable (reducible) property of PtO_x, which was reduced by the repetitive CV applications. In previous work [22–24], the oxidation and reduction on the Pd metal reduced from PdO are much easier than on normal bulk Pd, and similar results are found in Fig. 2. Thus, the

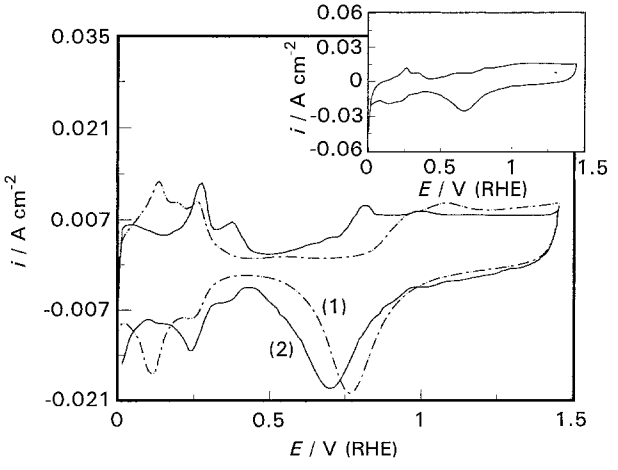

Fig. 2. Cyclic voltammograms at 50 mV s^{-1} for (a) type II PtO_x electrodes in (1) 0.5 M H_2SO_4 and (2) 1 M NaOH; and (b) type I PtO_x electrode in 1 M NaOH at 25 °C.

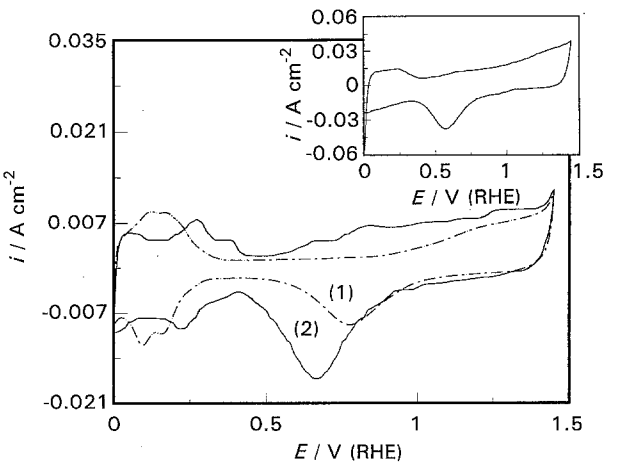

Fig. 3. Cyclic voltammograms at 50 mV s^{-1} for (a) type II electrodes in (1) 0.5 M H_2SO_4 and (2) 1 M NaOH; and (b) a type I electrode with 60 mol % Pt in precursors in 1 M NaOH at 25 °C.

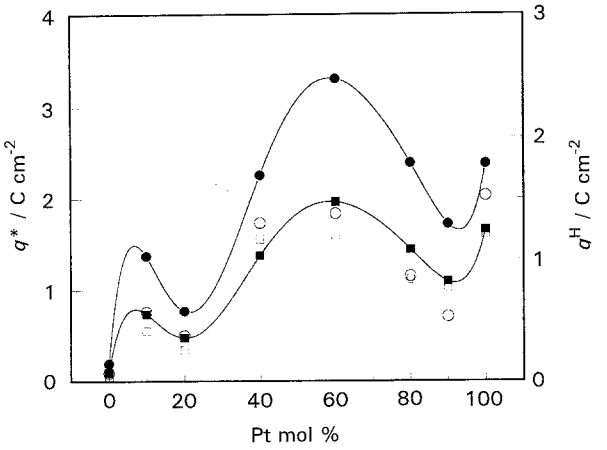

Fig. 4. Voltammetric charges of redox transitions (q^*, 1, 2) and hydrogen adsorption/desorption (q^H, 3, 4) for type II electrodes as a function of coating solution Pt content in (1, 3) 0.5 M H_2SO_4 and (2, 4) 1 M NaOH. Key: (●) q^* (base); (○) q^* (acid); (■) q^H (base); (□) q^H (acid).

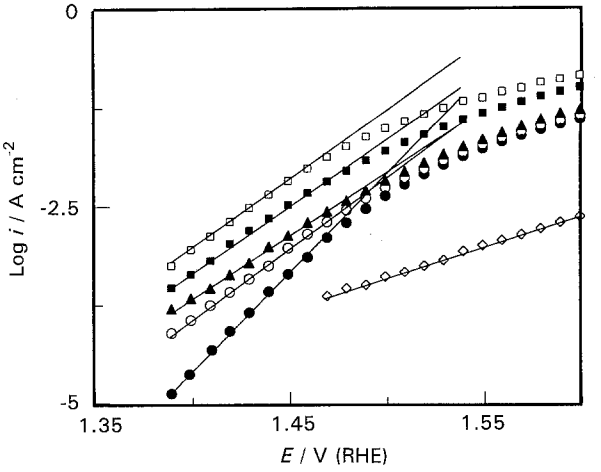

Fig. 5. Log i/E curves on type I electrodes in 0.5 M H_2SO_4. Scan rate: 0.5 mV s^{-1}. Pt content of coating solution is: (●) Ru_2; (○) 10%; (■) 40%; (□) 60%; (▲) 90%; (◇) PtO_x.

voltammetric currents on this mixed-oxide electrode are mainly due to Pt oxidation/reduction and hydrogen desorption/adsorption. In addition, the voltammetric responses of this series of Ru + Pt oxide electrodes are similar in shape to those in Fig. 2 and their voltammetric currents are larger than those of the RuO_2 electrode. These results reveal the instability of PtO_x. It is worth noting here that oxides of platinum group metals are unstable in the hydrogen adsorption/desorption region [25]. This is supported by the CVs of the PtO_x and PdO_y electrodes. In contrast, RuO_2, IrO_2, RhO_2 and OsO_2 electrodes are quite stable under repetitive cycling between the oxygen and hydrogen evolving regions. This is especially true of RuO_2 and IrO_2 which were employed as cathodes for the HER [13, 26].

The voltammetric charges of oxide formation/reduction in the 1.4–0.4 V region and hydrogen adsorption/desorption in 0.4–0 V on the CV curves of type II Ru–Pt oxides were obtained by numerical integration. These results are shown in Fig. 4 as a function of Pt mol % in precursors. The voltammetric charges of oxide formation/reduction and hydrogen adsorption/desorption, in general, increase with increasing Pt content, reach a maximum around 60 mol %, and decrease gradually with increasing Pt content with the exception of the PtO_x electrode. This indicates that the oxyplatinum sites involving redox transitions can be increased by mixing RuO_2 and PtO_x. The occurrence of a maximum activity was also found for the Ru–SnO_2 [27], Ir–RuO_2 [9, 13], Ni–Co oxide [28], etc. This may be due to (i) numerous defects in the mixed oxides, (ii) degree of dispersion of the PtO_x within the oxides, (iii) variation in surface roughness, and (iv) the electronic structure of the deposits. Thus, many mixed-oxide electrocatalysts have been investigated in the literature [9].

3.2. *Tafel studies for the oxygen and chlorine evolution reactions*

Tafel studies for the OER on a series of type I Ru–Pt oxide electrodes were carried out in 1 M NaOH and 0.5 M H_2SO_4. Typical results for H_2SO_4 are shown in Fig. 5. The Tafel plots, similar to those previously reported [13, 14], possess a change in Tafel slope from 60 to 120 mV decade^{-1} at 1.47 V with the exception of the PtO_x electrode. This phenomenon was attributed to a combination of three effects: (i) surface sites blocked by gas bubbles; (ii) a new rate-determining step predominating in the region of high current density; and (iii) a change in mechanism. The Tafel slope in the low overpotential region increases with increasing Pt content in the precursors (Table 1). This result is different from those of the mixed oxides with synergistic effects, since the dependence of Tafel slope for the OER on oxide composition indicates the degree of intimate mixing of two/three components [9]. In this work the starting current density (denoted hereafter as i_s) of these mixed-oxide electrodes was obtained by extrapolating the linear Tafel region to 1.35 V, which is close to the decomposition potential of water on RuO_2. The sequence of electrodes with respect to decreasing i_s, an index of the number of active sites: Ru–Pt oxide with 60 mol % Pt (128.8 μA cm^{-2}) > 40 mol % Pt (58.9 μA cm^{-2}) > 90 mol % Pt (39.8 μA cm^{-2}) > pure PtO_x (28.2 μA cm^{-2}) > 10 mol % Pt (13.2 μA cm^{-2}) > RuO_2 (1.6 μA cm^{-2}), however, is not consistent with the voltammetric charge data. This may be due to the fact that the decomposition potentials of oxygen evolution

Table 1. Tafel slope of the oxygen and chlorine evolution reactions at Ru–Pt binary electrodes

Pt content/mol %	*Tafel slope*/mV decade^{-1}	
	O_2	Cl_2
0	47.98	55.83
10	57.78	39.09
40	59.81	34.77
60	58.48	34.57
90	63.45	35.19
100	111.7	38.55

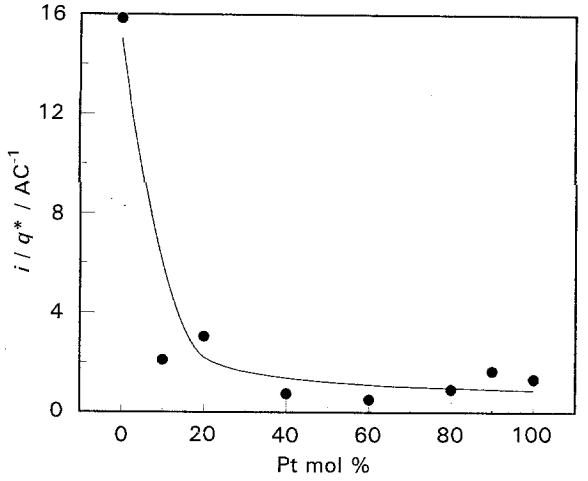

Fig. 6. Specific activities (i/q^*) of Ru–Pt oxides as a function of coating solution Pt content in 0.5 M H_2SO_4. Current density, i, was obtained from Tafel plots at 1.6 V.

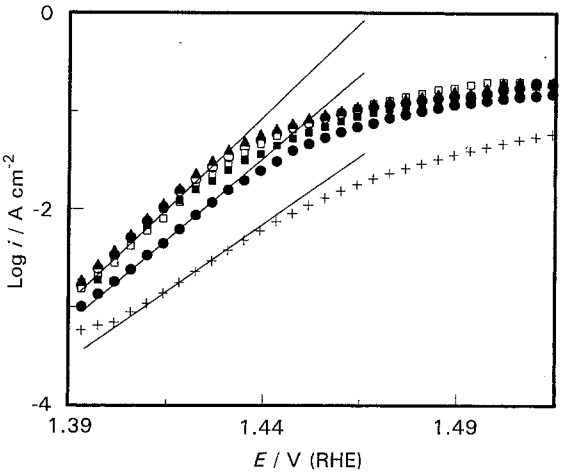

Fig. 7. Log i/E curves on type I electrodes in 3 M NaCl + 0.01 M HCl. Scan rate is 0.5 mV s^{-1}. Pt content of coating solutions is: (+) RuO_2; (■) 10% mol %; (○) 40% mol %; (▲) 70% mol %; (□) 90 mol %; (●) PtO_x.

on RuO_2 and PtO_x are different. Furthermore, the sequence of electrode with respect to decreasing current density at 1.6 V (i.e. at high OER overpotentials): Ru + Pt oxide with 60 mol % Pt (120.5 mA cm^{-2}) > 40 mol % Pt (102.1 mA cm^{-2}) > 90 (54.9 mA cm^{-2}) ≃ 10 (50.5 mA cm^{-2}) ≃ RuO_2 (46.3 mA cm^{-2}) > PtO_x (2.7 mA cm^{-2}) is not consistent with that of q^*, either. This is due to the fact that the oxygen evolving mechanisms/rate-determine steps on RuO_2 and PtO_2 are different (see Tafel slope data in Table 1). Based on the above results, voltammetric charge (q^*) can not be considered as a good index in estimating the suitability for OER of the Ru–Pt binary oxide system, although both q^* and the Tafel study reveal that the occurrence of maximum activity is at the electrode with Pt 60 mol %.

The specific activities (i/q^*) of various Ru–Pt oxides for the OER [9], where i is obtained at 1.6 V from the Tafel plots, are shown in Fig. 6 as a function of Pt content in the precursors. The specific activity of Ru–Pt oxide decreases sharply and becomes approximately constant as the platinum content increases; a result indicative of two facts. First, platinum oxide is not a good electrocatalyst for the OER. Secondly, the mixing of RuO_2 and PtO_x does not take place at atomic scale and thus, does not possess synergistic effects for this reaction. Since synergistic effects often occur when two/three components are under atomic mixing [9], this does not occur for the Ru + Pt binary oxide system, possibly due to the fact that RuO_2 is a rutile structure while PtO_x is not [29, 25]. On the other hand, although synergistic effects for oxygen evolution on the Ru + Pt oxides do not occur, this result is possibly favourable to CER because of the depression of OER.

The Tafel plots for the CER on a series of type I Ru–Pt oxide electrodes in 3 M NaCl + 0.01 M HCl solution at 25 °C, are shown in Fig. 7. The Cl_2 evolving rate on RuO_2 is lowest in the whole investigated potential region but is similar on the Ru–Pt oxides at electrode potential above 1.44 V. The Tafel slope of CER (Table 1), in general, is constant (~40 mV decade^{-1}), with the exception of RuO_2 (60 mV decade^{-1}), implying that the mechanisms of CER on the binary electrodes are the same. These results are possibly due to the fact that the CER only occurs on the external surface [1] since this reaction has a low activation overpotential (i.e. a relatively reversible reaction). Based on the Tafel results of both OER and CER, the electrodes with platinum content from 10–20 mol % ought to have an optimal current efficiency for CER/hypochlorite production since they have low oxygen and high chlorine gas evolving rates, respectively.

3.3. *Current efficiency of hypochlorite production*

Hypochlorite producing efficiencies on type I Ru–Pt oxide-coated electrodes are presented as a function of current density in Fig. 8. In general, current efficiency reaches a maximum at about 300 mA cm^{-2}. On the other hand, it decays gradually on the pure

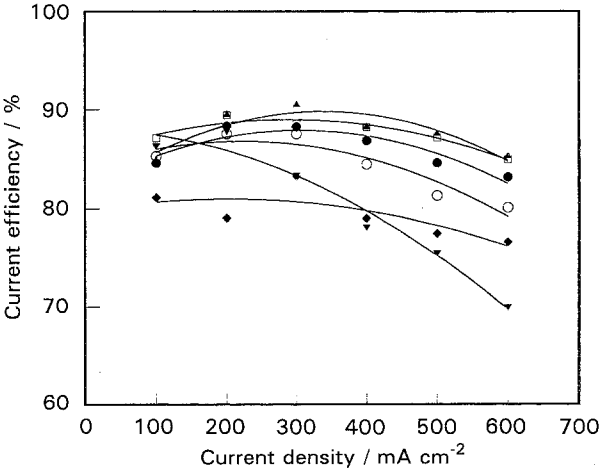

Fig. 8. Current efficiencies of type I Ru–Pt oxides for hypochlorite production as a function of current density in 0.5 M NaCl solution. Platinum content: (◆) RuO_2; (▲) 20 mol %; (□) 40 mol %; (●) 60 mol %; (○) 80 mol %; (▼) PtO_x.

oxide-coated electrodes, especially the PtO_x electrode. For the Ru + Pt binary oxide electrodes, the current efficiency of hypochlorite production decreases with increasing Pt content. The maximum current efficiency, 91.7%, was obtained on the Ru + Pt oxide electrode with 20 mol % Pt in the precursor at 300 mA cm^{-2}. This result indicates that the oxygen chlorine evolution rate on RuO_2 can, respectively, be depressed and enhanced by the presence of minor amounts of PtO_x.

3.4. *Surface morphologies and element mapping*

Since the hypochlorite producing/chlorine evolving rates are strongly dependent on the external surface of different electrodes, surface morphologies of this series of Ru–Pt oxide electrodes were examined. Typical SEM photographs of Ru–Pt oxide electrodes with precursor Pt mol % of 0, 20, 60, 80,100 are shown in Fig. 9 as (a), (b), (c), (d) and (e), respectively. In general, the surface morphologies of these electrodes are

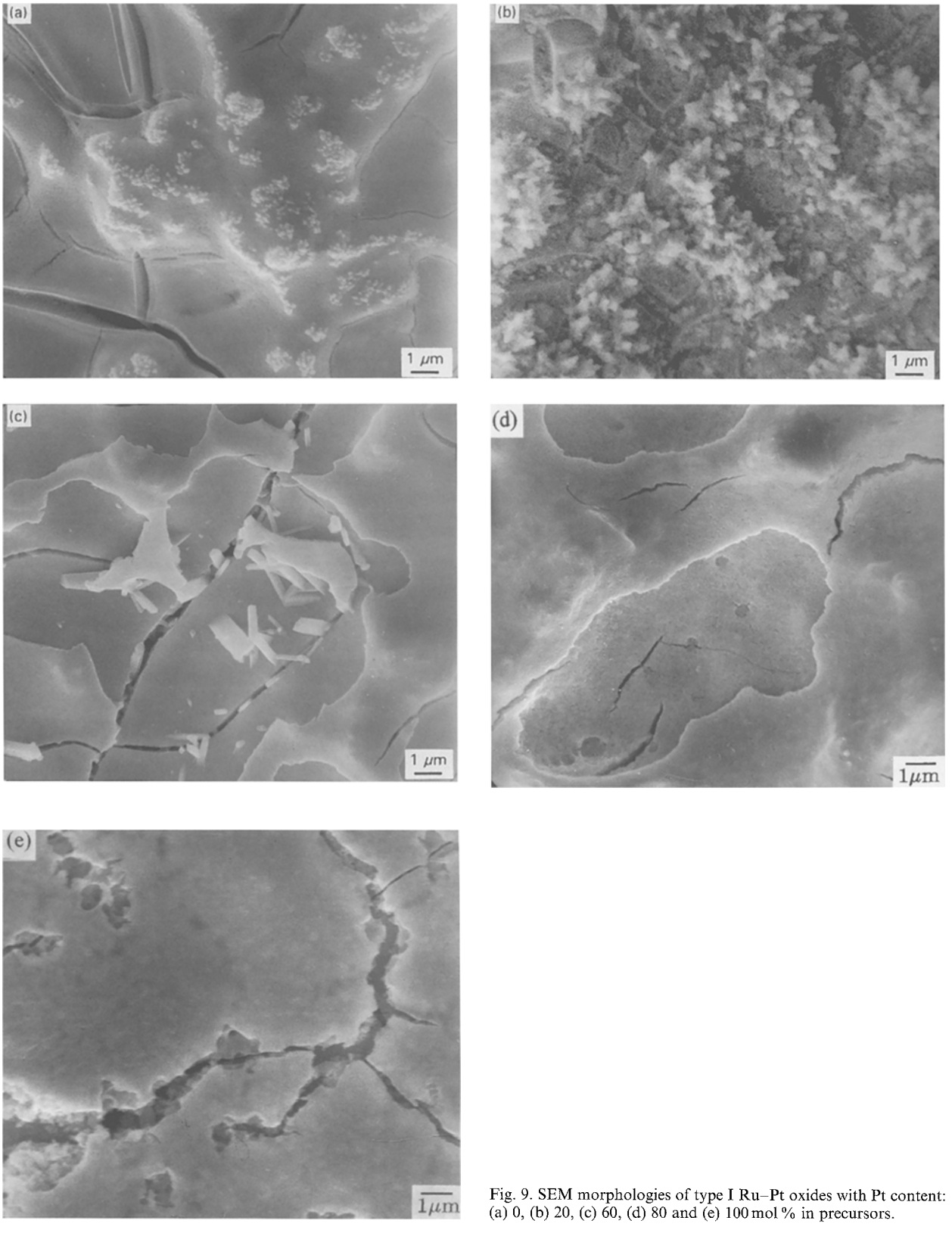

Fig. 9. SEM morphologies of type I Ru–Pt oxides with Pt content: (a) 0, (b) 20, (c) 60, (d) 80 and (e) 100 mol % in precursors.

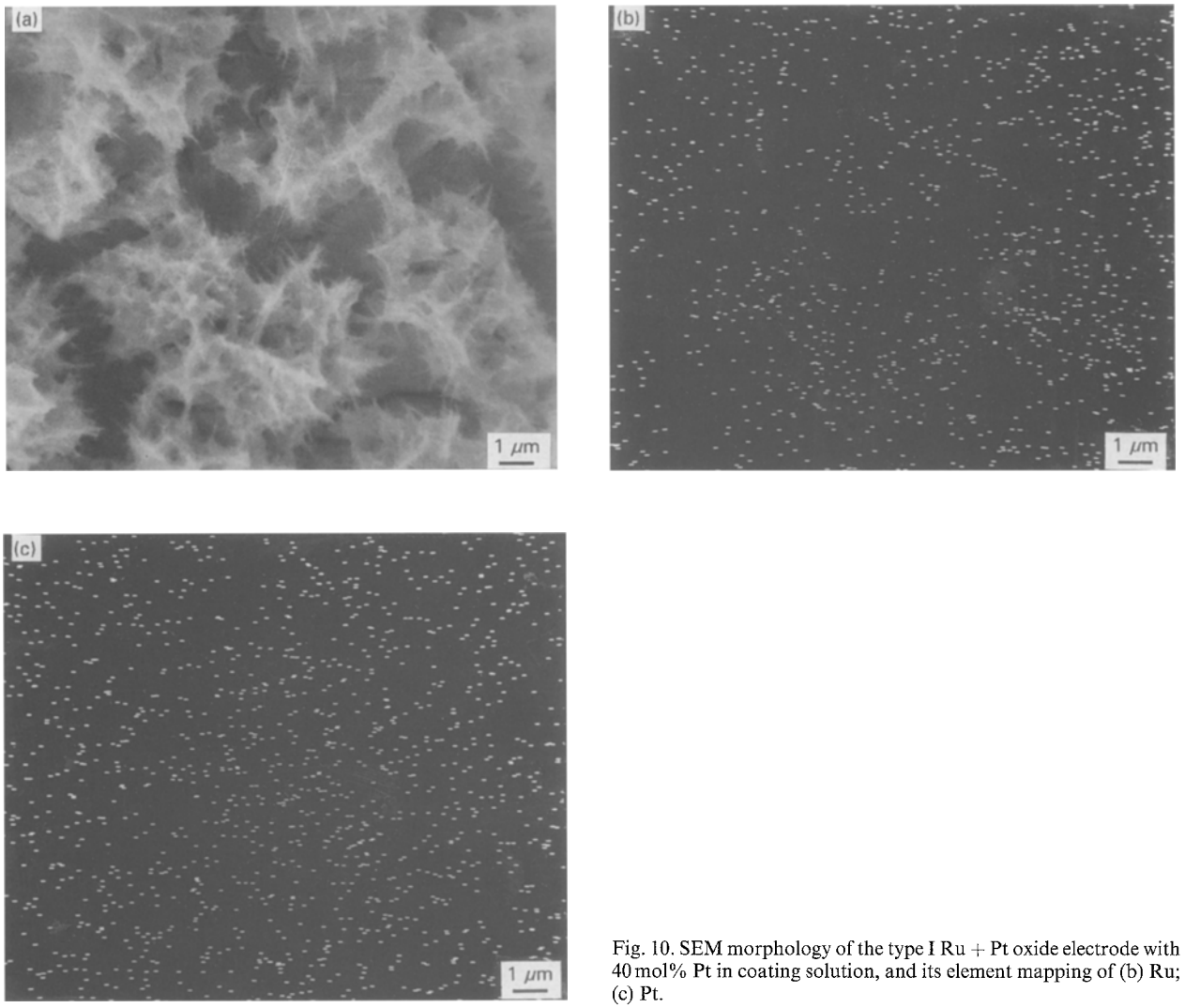

Fig. 10. SEM morphology of the type I Ru + Pt oxide electrode with 40 mol% Pt in coating solution, and its element mapping of (b) Ru; (c) Pt.

not very porous but several surface cracks are observed. Therefore, the Cl_2 evolution rates on these electrodes are approximately the same (see Tafel results in Fig. 7). Note that the surface of the Ru + Pt oxide electrodes with 20–40 mol % Pt, is covered by a thin layer of variegated material. This suggests that RuO_2 and PtO_x are not well-mixed.

To check the distribution of Pt and Ru on the oxide, element mapping of Ru and Pt was examined. Figure 10 shows both the surface morphology and element mapping of the Ru + Pt oxide electrode with 40 mol % Pt. The variegated material also can be found on the surface of this electrode from the SEM photograph. Pt is dispersed homogeneously while Ru is enriched on the variegated material. This reveals that RuO_2 and PtO_x are repulsive to each other and phase segregation occurs. Therefore, from the Tafel slope and element mapping results, it is reasonable to conclude that no synergistic effects for the OER on the Ru + Pt binary oxide electrodes are caused by phase segregation between these two oxides.

3.5. *Effects on the repetitive CVs pretreatment*

Hypochlorite producing efficiencies on type I Ru + Pt oxide electrodes with 20 and 60 mol % Pt are presented as a function of current density in Fig. 11 as curves 1 and 2, respectively. Also, curves 3 and 4 shown in Fig. 11 are their respective current efficiencies on the type II electrodes. On all curves, hypochlorite producing efficiency reaches a maximum at 300 mA cm^{-2} whether or not the electrodes have been cycled. The current efficiencies of the electrode with 20 mol % Pt (i.e. curves 1 and 3) are respectively higher than those of the electrode with 60 mol % Pt (curves 2 and 4). Note that the current efficiencies on these two type II electrodes are respectively higher than on their corresponding type I electrodes, indicating that RuO_2+ Pt is more favourable for the CER.

To clarify the above effects, OER and CER on both type I and II electrodes were investigated by Tafel study. Typical Tafel plots for the OER and CER on type I and II Ru + Pt oxide electrodes with 60 mol % Pt are shown in Fig. 12. A comparison of curves 1 and 2 for the OER indicates that this reaction is significantly depressed on the type II electrode. In addition, from an examination of curves 3 and 4, the Cl_2 evolution rate on the type II electrode is much higher than that on the type I electrode. In comparison to type I electrode, the increase in chlorine evolving activity and decrease in oxygen evolving activity on type II electrode also occurs for the

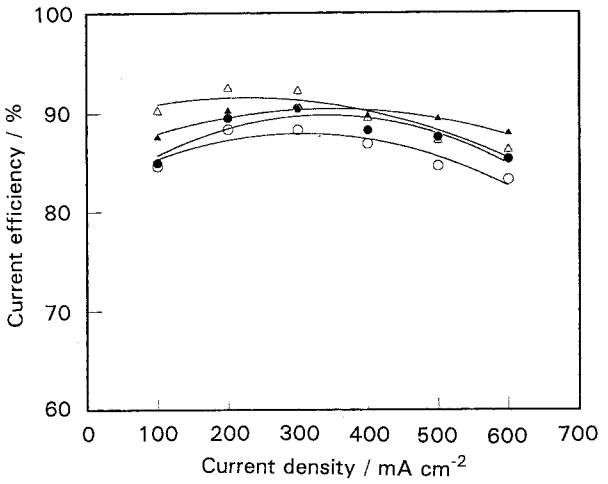

Fig. 11. Current efficiencies of Ru + Pt oxides with Pt content equal to (1, 3) 20 and (2, 4) 40 mol % for hypochlorite production as a function of current density in 0.5 M NaCl solution. (1, 2) and (3, 4) are for type I and II electrodes, respectively.

PtO_x electrode, while a minor increase in the oxygen evolution rate is found on the type II RuO_2 electrode. The former result implies that (i) Pt reduced from PtO_x has a rougher external surface because of the place-exchange reaction in the Pt oxide reduction; and (ii) the Pt reduced from PtO_x has a lower activity for the OER. The latter inference is supported by the fact that the oxygen evolution rate/mechanisms on Pt are affected by the presence of Pt oxides [30]. The latter result is attributed to the increase in active sites and hydrophilicity of the RuO_2 produced by repetitive cycling [9].

The surface morphologies of the type II Ru–Pt oxide electrodes were examined by scanning electron microscopy. Typical SEM photographs for the electrodes with Pt 0, 20, 40, 60, 80, 100 mol % are shown in Fig. 13(a)–(f), respectively. The surface morphologies are very rough with many cracks. A comparison of Figs 13 and 9 reveals that type II electrodes have

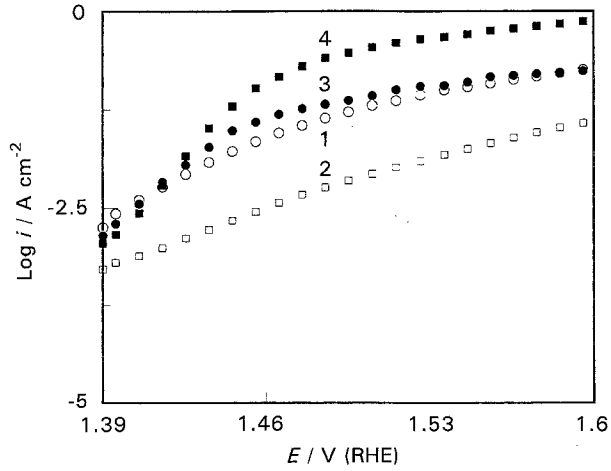

Fig. 12. Log i/E curves for (1, 2) oxygen evolution and (3, 4) chlorine evolution on the Ru + Pt oxide electrode with 60 mol % Pt in 0.5 M H_2SO_4 and 3 M NaCl + 0.01 M HCl solution, respectively. (1, 3) and (2, 4) are for type I and II electrodes, respectively. Scan rate: 0.5 mV s^{-1}.

rougher surfaces than type I electrodes; this is especially true of binary Ru + Pt oxide and PtO_x electrodes. This supports the inference that the place-exchange reaction during Pt oxide reduction yields a rougher surface on type II electrodes. A comparison of Figs 13(b), (c), 9(b) and 10(a) reveals that the variegated structure of Ru-enriched material is more obvious on type II electrodes. This is possibly due to repulsion between RuO_2 and PtO_x during the reduction process. This more obvious segregation of RuO_2 and Pt phases also explains the higher current efficiencies of hypochlorite production on the type II Ru + Pt oxide electrodes.

From the above results, the fact that current efficiencies of the hypochlorite production on type II electrodes are higher than on type I electrodes is due to: (i) Pt reduced from PtO_x depresses the OER more significantly in comparison to its corresponding oxide and (ii) the CER on a RuO_2 + Pt electrode is more favoured than on a Ru + Pt oxide electrode.

To clarify the effect of repetitive cycling on the distribution of Pt and Ru oxides, and depth profile of Pt, Ru, Ti, and O within the coating matrix was determined by Auger electron spectroscopy (AES). Typical results of both type I and II electrodes with 40 mol % Pt are shown in Fig. 14(a) and (b), respectively. In both figures, curves 1, 2, 3 and 4 are indicative of Pt, Ru, O and Ti, respectively. Ruthenium dioxide has migrated into the inner layer of the oxide coating and the titanium/oxide interface in Fig. 14(a). This is due to the fact that the crystalline structure of RuO_2 and TiO_2 is rutile [25, 29, 31, 32] and, accordingly, Pt is the surface-enriched component. The O count gradually increases in the initial 10 ks, reaches a maximum at about 1.5×10^4 seconds, and decreases more quickly in the 20–25 ks region. In fact, most oxide coatings usually possess bulk oxygen deficient and surface oxygen excess phenomena because of the final annealing in air [33, 34]. The above result indicates that during electrode preparation, several Pt(IV) atoms were reduced to PtO and Pt because isopropanol (precursor solvent) may be oxidized by Pt(IV) species, especially at high temperature (e.g. during drying and pyrolysis processes) [35]. A comparison of Fig. 14(a) and (b) reveals that PtO_x has been reduced to Pt by the cycling since the count of oxygen is smaller in Fig. 14(b). In addition, the oxygen count also reaches a maximum at about 15 ks indicating that RuO_2 is not reduced by cycling. Since the surface-enriched phenomenon of the Pt atoms is more obvious in Fig. 14(b), the speculation that during reduction of PtO_x, RuO_2 is repelled from the lattice matrix of Pt is reasonable.

3.6. *Stability testing for hypochlorite production*

Typical results of stability testing for the type II electrode with 20 mol % Pt are shown in Fig. 15. The cell voltage increased gradually with electrolysis time since Cl^- ions were consumed by the hypochlorite production. On the other hand, the value of cell

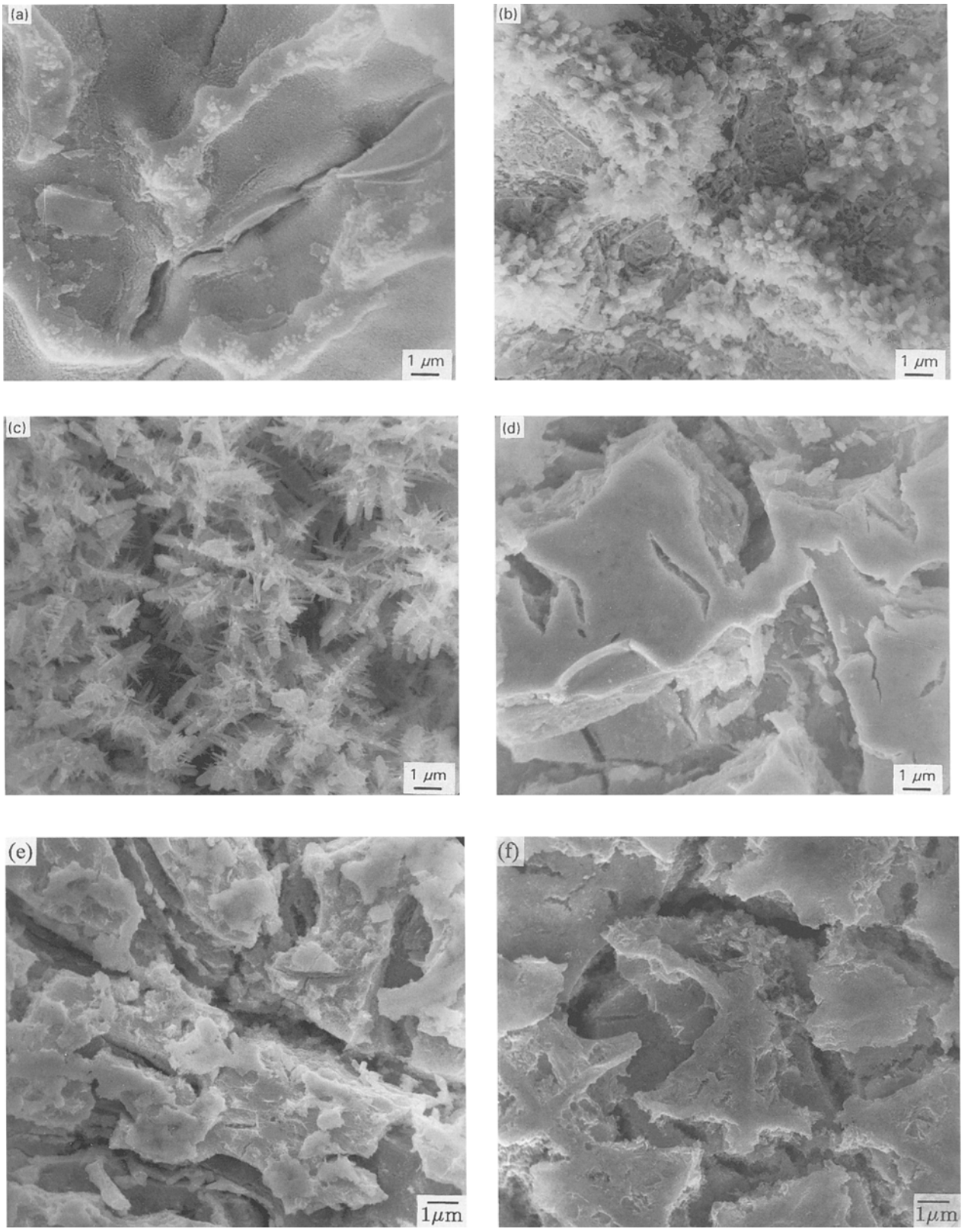

Fig. 13. SEM morphologies of type II Ru–Pt oxides. The Pt content is (a) 0, (b) 20, (c) 40, (d) 60, (e) 80 and (f) 100 mol %.

voltage decreased sharply to its initial value (5.3 V) when the electrolytes were renewed. This phenomenon is not affected by the interuption of electrolysis, indicating that these electrodes are very stable under the above conditions. Therefore, the reduction of PtO_x to Pt does not decrease the service life of the Ru + Pt binary system.

4. Conclusion

Cyclic voltammetric results indicated that PtO_x was reduced to Pt under repetitive cyclic voltammety in the potential region between HER and OER. The maximum activity of the Ru + Pt oxide electrodes for the OER was located at about 60 mol % Pt in

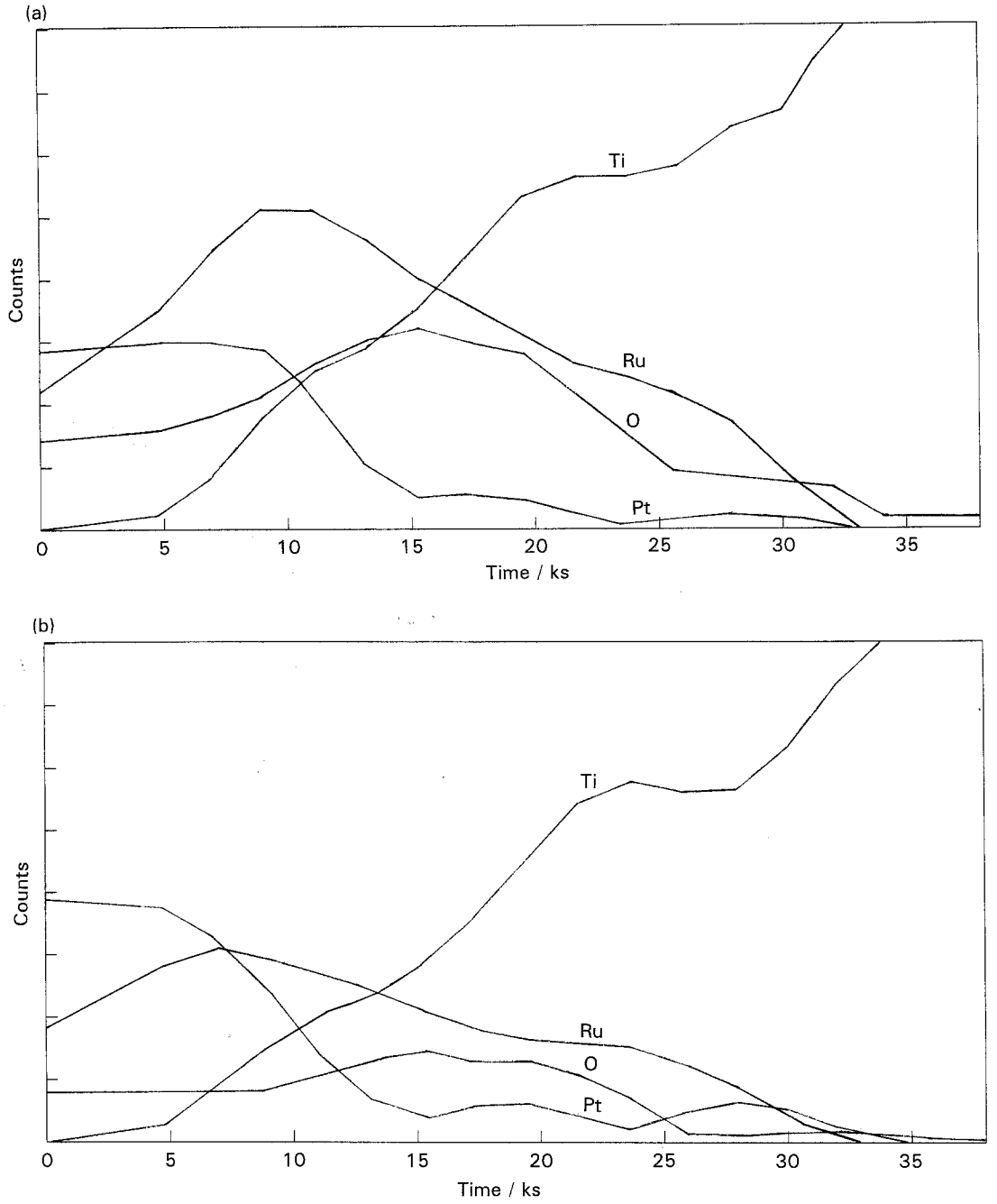

Fig. 14. An Auger depth profile of Ru, Pt, Ti and O from (a) type I and (b) type II Ru + Pt binary electrodes with 40 mol % Pt in precursors.

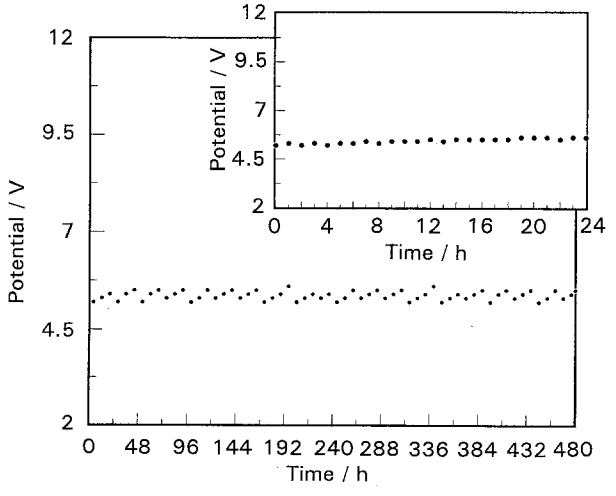

Fig. 15. Stability of the type II Ru + Pt binary electrode with 20 mol% Pt in precursors.

the precursors from both the voltammetric charges and Tafel studies. The specific activities and Tafel slopes of these mixed oxide electrodes, respectively decreasing and increasing with increasing the Pt content, revealed that mixing of the RuO_2 and PtO_x had no synergistic effects for the OER. The hypochlorite producing efficiency reached a maximum on the electrode with 20 mol % Pt. SEM photographs and element mapping revealed poor mixing of $RuO_2 + PtO_x$ and RuO_2 + Pt crystallites. AES results revealed that Pt is the surface-enriched element on both type I and II electrodes. Stability testing of type II electrodes indicated that the reduction of PtO_x to Pt does not decrease the service life of the Ru + Pt binary system. In comparison to type I electrodes, the reasons for a higher rate/current efficiency of the CER/hypochlorite production on type II electrodes are: (i) Pt reduced

from PtO_x on the Ru + Pt oxide electrodes depressed the OER and (ii) rougher external surfaces of the RuO_2 + Pt electrodes are more favourable for the CER.

Acknowledgement

The financial support of this work by the National Science Council of the Republic of China under contract NSC 84-2214-E006-004 is gratefully acknowledged.

References

[1] H.-J. Heidrich, L. Muller and B. I. Podlovchenko, *J. Appl. Electrochem.* **20** (1990) 686 and reference cited therein.
[2] S. Trasatti, *Electrochim. Acta* **32** (1987) 369.
[3] J. A. Harrison, D. L. Caldwell and R. E. White, *ibid.* **28** (1983) 1561.
[4] *Idem, ibid.* **29** (1984) 203.
[5] H. B. Beer, *US Patent 3 711 385.*
[6] K. J. O'Leary, *US Patent 3 776 834.*
[7] S. Saito, K. Aue and N. Shimojo, *US Patent 4 061 558.*
[8] H. B. Beer, *US Patent 4 425 2117.*
[9] S. Trasatti, *Electrochim. Acta* **36** (1991) 225.
[10] F.-B. Li, A. R. Hillman and S. D. Lubetkin, *ibid.* **37** (1992) 2715.
[11] T. A. F. Lassali, J. F. C. Boodts, S. C. de Castro, R. Landers and S. Trasatti, *ibid.* **39** (1994) 95.
[12] '*Standard Methods for the Examination of Water and Wastewater*', APHA 16th edn. (1985) p. 426.
[13] T.-C. Wen and C.-C. Hu, *J. Electrochem. Soc.* **139** (1992) 2158.
[14] L. D. Burke and J. F. O'Neill, *J. Electroanal. Chem.* **101** (1979) 341.
[15] R. Kötz and S. Stucki, *Electrochim. Acta* **31** (1986) 1311.
[16] L. D. Burke and O. J. Murphy, *J. Electroanal. Chem.* **96** (1979) 19.
[17] S. F. Cogan and R. D. Rauh, 'Large-Area Chromogenics: Materials and Devices for Transmittance Control' (edited by C. M. Lampert and C. G. Granqvist), SPIE Institutes for Advanced Optical Technologies **4** (1988) 482.
[18] L. D. Burke and M. B. C. Roche, *J. Electroanal. Chem.* **259** (1983) 89.
[19] A. A. El-Shafei, S. A. Abd. El-Maksoud and M. N. H. Moussa, *ibid.* **336** (1992) 73.
[20] L. D. Burke and K. J. O'Dwyer, *Electrochim. Acta* **34** (1989) 1659.
[21] L. D. Burke, J. K. Casey and J. A. Morrissey, *ibid.* **38** (1993) 897.
[22] C.-C. Hu and T.-C. Wen, *J. Electrochem. Soc.* **142** (1995) 1376.
[23] *Idem., Electrochim. Acta* **40** (1995) 495.
[24] T.-C. Wen and C.-C. Hu, *J. Electrochem. Soc.* **140** (1993) 998.
[25] S. Trasatti and G. Lodi, 'Electrodes of Conductive Metallic Oxides, Part A' (edited by S. Trasatti), Elsevier, Amsterdam (1980) p. 301.
[26] J. C. F. Boodts and S. Trasatti, *J. Appl. Electrochem.* **19** (1989) 255.
[27] M. E. G. Lyons and L. D. Burke, *J. Chem. Soc. Faraday Trans. 1* **83** (1987) 299.
[28] C.-C. Hu, Y.-S. Lee and T.-C. Wen, *J. Electrochem. Soc.* submitted.
[29] J. F. C. Boodts and S. Trasatti, *J. Electrochem. Soc.* **137** (1990) 3784.
[30] A. E. Bolzan and A. J. Arvia, *J. Electroanal. Chem.* **375** (1994) 157.
[31] F. Hine, M. Yasuda and T. Yoshida, *J. Electrochem. Soc.* **124** (1977) 500.
[32] W. A. Gerrard and B. C. H. Steele, *J. Appl. Electrochem.* **8** (1978) 417.
[33] J. Augustynski, L. Balsenc and J. Hinden, *J. Electrochem. Soc.* **125** (1978) 1093.
[34] L. C. Schumacher, I. B. Holzhueter, I. R. Hill and M. J. Dignam, *Electrochim. Acta* **35** (1990) 975.
[35] N. Kamiya, M. Obara, K.-I. Ota, T. Takata and T. Endo, *Denki Kagaku* **60** (1992) 467.